JOURNAL OF MATERIALS SCIENCE 33 (1998) 3975–3984

Influence of voids on the stress distribution and deformation behaviour of epoxies under uniaxial deformation

C. FOND
CNRS, Institut Charles Sadron, 6 rue Boussingault, F-67083 Strasbourg, France
J. KIEFER, D. MENDELS, J.B. FERRER, H.H. KAUSCH, J.G. HILBORN
Swiss Federal Institute of Technology, Materials Department, Polymers Laboratory, CH-1015 Lausanne, Switzerland
E-mail: fond@ics.u-strasbg.fr

A zero-order model is presented, which allows calculation of the stress distribution in porous epoxies by taking into account the interaction between randomly distributed voids. These results demonstrate that the mean value of the stress concentration factor increases with the volume fraction of voids. This leads to a decrease in sample yield strength. However, the generation of a porous morphology also creates a considerable number of regions where the stress is completely released. The theoretical predictions are in good agreement with experimental results obtained with macroporous epoxies, which were prepared based on the chemically induced phase separation technique, and tested under uniaxial compression. © *1998 Kluwer Academic Publishers*

1. Introduction

Voids often develop during the synthesis and processing of metals, ceramics, polymers and composites. These isolated pores are usually regarded as inhomogeneities, which act as stress concentrators and consequently initiate plasticity or failure in materials. Thus the presence of such voids causes severe problems concerning the reliability of mechanical properties, such as the toughness, modulus and yield strength. A completely different behaviour might result, if the voids are numerous, have a very uniform size, and are randomly dispersed in an isotropic matrix in such a manner, that the resulting stress fields can interact. The development of such a morphology has been recognized in highly cross-linked polymers, where a dispersed phase is able to cavitate during deformation [1–10]. This cavitation is accompanied by the extensive formation of shear bands, which leads to energy absorption and consequently a higher toughness. Even though the incorporation of second-phase particles is a well established method to increase the toughness of otherwise brittle thermosets [11–14], there still exists a controversial discussion, whether the cavitation is only a side symptom [15, 16], or if it is at the origin of the shear banding [1, 4–6, 9, 17]. Numerous experimental observations confirm the latter hypothesis.

The understanding of the cavitation process becomes crucial to develop new materials, combining high specific properties with increased toughness. The nature of second-phase particles does not always seem to play the predominant role for toughening. A wide variety of thermoplastic or rubbery particles, that are generated via reaction-induced phase separation are mostly used for these purposes [98, 11–14]. The desired toughening effect can also be achieved by using highly branched polymers, phase separating to dispersed domains [18] or alternatively by blending with a wide variety of core shell particles [19]. However, the size and distribution of the second phase seems to be crucial for effective toughening. Several groups observed that no toughening occurs if the second-phase particles are smaller than 200 nm [5, 7]. Theoretical calculations have shown that this is a lower critical size to induce cavitation [20] and that a cavitated particle can generally be considered as a void [21, 22]. Multiple cavitation is equal to the generation of a series of voids. Hence, several attempts have been made to simulate such a morphology by using either a non-reactive rubber [17] or hollow latex spheres [23, 24] as the dispersed phase. Based on the theoretical predictions and the experimental results, it was concluded that voids are able to toughen epoxies in the same manner and in the same magnitude as rubber particles. Furthermore, the contribution of the plastic void growth, succeeding cavitation, to the total toughness can become as important as shear band formation, especially at elevated temperatures [25]. Furthermore, it has been observed that rubber particles become ineffective in toughening if the cavitation is suppressed under a hydrostatic pressure [26]. Consequently, cavitation has been regarded as a prerequisite for toughening. However, rubber-toughened materials can undergo plasticity without cavitation at

low strain rate or high temperature [21, 22]. Hence rubber particles or voids must be seen as stress perturbators. According to the concept of Wu [27], the toughening depends not on the size of the particles, but on the interparticle distance. A substantial increase in toughness is only achieved if the interparticle distance becomes lower than a critical value. Later, this model has been refined by the same author supposing a percolation of matrix ligaments with a critical size, wherein shear bands are able to form [28]. Both explanations imply that the particles must be able to interact.

Very recently, a further interesting observation has been reported, which also suggests the importance of cavitation for toughening. Similar to the transformation-induced toughening, which is widely used for ceramic materials, Karger–Kocsis has tried to increase the toughness of polypropylene by the incorporation of crystalline particles which will undergo a phase transition during deformation [29, 30]. Conversely to the observations reported for ceramics, the toughness does not increase if this phase transition is accompanied by a volume increase, thus creating a compression field around the crack tip. However the toughness increases, if a volume contraction occurs. This process might be very similar to cavitation.

All the above considerations lead us to the idea of preparing macroporous thermosets having closed pores with sizes and distributions in the micrometre range similar to those commonly used for toughening with rubber or thermoplastic particles. Therefore, we have developed a new technology, termed chemically induced phase separation (CIPS), because the generation of the desired morphology is governed by a phase separation process resulting from a chemical quench [8]. In this strategy, the epoxy precursor and curing agent are cured in the presence of a low molecular weight liquid, which should turn into a non-solvent upon curing, thus initiating a phase separation. This process should result in the formation of liquid droplets, spherical in shape due to thermodynamic reasons. The generation of a porous morphology is subsequently achieved by diffusion of the liquid through the cross-linked matrix without any alteration in the size and distribution of the dispersed phase [31–34]. This new type of macroporous thermoset is characterized by a very narrow size distribution in the micrometre and a significantly lower density without any lowering in thermal stability. The first experimental results demonstrate the general feasibility of the CIPS technique to prepare solvent-modified epoxies with a substantial increase in fracture energy of around 400% [35].

It is the purpose of this paper to present calculations of the stress distribution in porous thermosets and compare these results with the deformation behaviour of macroporous epoxies which were prepared via the CIPS technique and display a morphology which is close to the theoretical simulations. Recently, the stress distributions of a limited number of spherical inclusions, being either rubber or voids, in an isotropic epoxy matrix were calculated based on a finite element model [36, 37]. It was concluded that the effect of voids or a rubbery phase is very similar. These inclusions will release the triaxial stresses at the crack tip. Even though this model has allowed prediction of the possibility of void toughening (as proved later experimentally with one single psueudo-porous system [17]), the finite element approach does not allow the multiple interactions between randomly distributed voids to be taken into account. Therefore, our approach starts with a zero-order approximation of the stress interaction as explained below.

2. Interactions between spherical voids in an elastic matrix: A zero order model

2.1. Principle of the computations

The spherical inhomogeneities are randomly placed in a linear isotropic elastic matrix. The computation is based on the superposition of mechanical fields. Each of these fields is obtained from Eshelby's solution [38, 39] for the problem of an elastic infinite matrix containing elastic ellipsoidal inhomogeneities. This method based on the strain tensor inside the inhomogeneities is analogous to the equivalent inclusion method based on the stress tensor inside the inhomogeneities, using the zero-order expansion of the Taylor series describing the eigenstrain inside the inhomogeneities [40]. In our case (in order to simplify the software) we have considered spherical inhomogeneities so that all functions can be analytically computed and the system of coordinates has the same angle for all inhomogeneities. As the solution for a spherical inhomogeneity leads to a uniform strain tensor in the inhomogeneity, the solution involves the superposition of uniform strain tensors inside the inhomogeneities. The strain or stress values inside the inhomogeneity are then composed of a constant value in addition to the perturbations arising from the neighbouring inhomogeneities.

In order to obtain a linear system of equations describing the mechanical interactions, one considers the remote uniform strain of the matrix around each inhomogeneity. The six components of this remote strain tensor are then the unknowns attached to each inhomogeneity. The main effect on the solicitation of each inhomogeneity arises from the external loading. The local perturbation to this "mean field" is due to the interaction with the neighbouring inhomogeneities

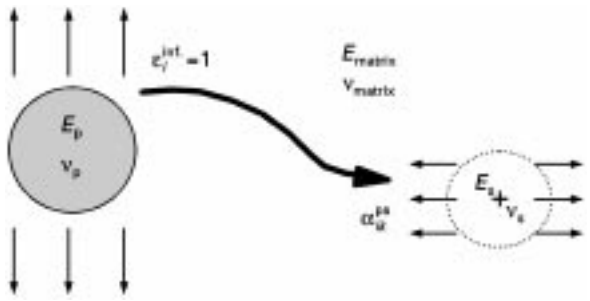

Figure 1 Effect of the p inhomogeneity on the s inhomogeneity. The component i of the remote strain tensor ε_i^{inf} acting on p induces a mean strain in the area occupied by s. The coefficient of influence α_{ki}^{ps} is attached to the component k of this mean strain tensor acting on s.

(Fig. 1). Of course this scheme is expected to give imprecise results when the inhomogeneities are very close to each other. Indeed, in such cases these perturbations vary considerably within the volume occupied by the inhomogeneity and thus cannot be considered almost uniform (zero-order approximation). It is expected that the zero-order approximation will give good results if the distances between inhomogeneities are relatively large. This will be checked below.

The six unknowns per inhomogeneity are then computed from the following system of equations

$$\varepsilon_i^{\mathrm{p}} = \varepsilon_i^{\infty} + \sum_{k=l}^{6} \sum_{s=1, s\neq p}^{n_v} \alpha_{ki}^{\mathrm{ps}} \varepsilon_k^{\mathrm{s}} \qquad (1)$$

where n_v is the number of inhomogeneities, ε_i^{∞} is the component i of the strain tensor applied at infinity, $\varepsilon_i^{\mathrm{p}}$ is the component i of the strain tensor acting on the p inhomogeneity considered alone in an infinite matrix, $\varepsilon_k^{\mathrm{s}}$ is the component k of the strain tensor acting on the s inhomogeneity considered alone in the same infinite matrix, $\alpha_{ki}^{\mathrm{ps}}$ represents the perturbation on ε_k arising from the presence of p at the centre of the location of s. The coefficient of influence, $\alpha_{ki}^{\mathrm{ps}}$ is analytically known for spheres [41, 42]. Once the solution is obtained $(\varepsilon_i^{\mathrm{p}}, \varepsilon_k^{\mathrm{s}}, \ldots)$ the stresses, strains and displacements can then be calculated (as in a boundary element technique) by superposition of the effects of $(\varepsilon_i^{\mathrm{p}}, \varepsilon_k^{\mathrm{s}}, \ldots)$, using Eshelby's solution for an inhomogeneity in an infinite matrix.

Each inhomogeneity has its own characteristics (elastic moduli, location and radius). For the sake of simplicity, in the following examples all the inhomogenetities have the same radius. As we were interested in porous materials, all inhomogeneities are voids. In fact, for numerical reasons, the Young's moduli of the inhomogeneities were set to be 10^{-6} times the Young's modulus of the matrix, which leads to the quasi exact situation of voids in the matrix.

2.2. Validations and limits of the zero-order approximation

It is obvious that the solution obtained by this procedure is exact for one inhomogeneity in an infinite matrix, but, as explained above, the zero-order approximation is expected to give imprecise stress concentration factors if several inhomogeneities are close together. To check the accuracy of the zero-order approximation it is necessary to compare results in cases of known solutions obtained by other techniques. Very few analytical results are available in the literature and generally the entire mechanical field is not explicitly given. The most convenient technique to obtain comparable fields would certainly be the boundary element technique. Nevertheless, we have used a finite element software applied to two-dimensional axisymetrical geometries. Once comparable fields are given, a criterion for the quality of the solutions must then be defined. We have chosen to compare the strain field and to evalute the difference between the two strains relative to the applied strain amplitude at infinity (the greatest value of ε_i). One of the most imprecise results is given in the case where inhomogeneities are voids, in triaxial tension or compression and for only two voids. In this case, the neighbouring voids imbalance the strains in such a way that they cannot be counterbalanced by a zero-order distribution of strains. Two voids of the same radius separated by a distance of one radius is the geometry shown in Fig. 2. The finite element software was ABAQUS/Standard© version 5.3. The mesh was axisymetric around the y-axis, symmetric to the x-axis and composed of six-node triangles. The cylinder containing the two spheres of radius r was of radius $4r$ and height $24r$ in order to approach as closely as possible the case of two spheres in a infinite medium. This mesh allows three cases to be studied uniaxial tension of axis y, bi-axial tension of axis x and z, and tri-axial tension.

The strains along four axes ($x = 0, x = r, y = 0, y = r/2$) are plotted in Fig. 3 in case of a triaxial strain of amplitude 1%. The maximum difference between the results from finite element and the present technique is encountered at the middle point between the voids. The error there is 27% of the applied strain "at infinity". In this zone, the strains seems to be overestimated by the present technique, i.e. the unloading in this zone due to the presence of two voids is underestimated. But we will focus our further discussions on strain and stress concentrations which are encountered in the vicinity of the voids. The strain fields around the voids have been computed for three different types of loadings at infinity: uniaxial tension, bi-axial tension and tri-axial tension (Fig. 4). The difference between the strain concentration factors is approximately 11%. We have then concluded that the separating distance between the spheres should not be lower than one

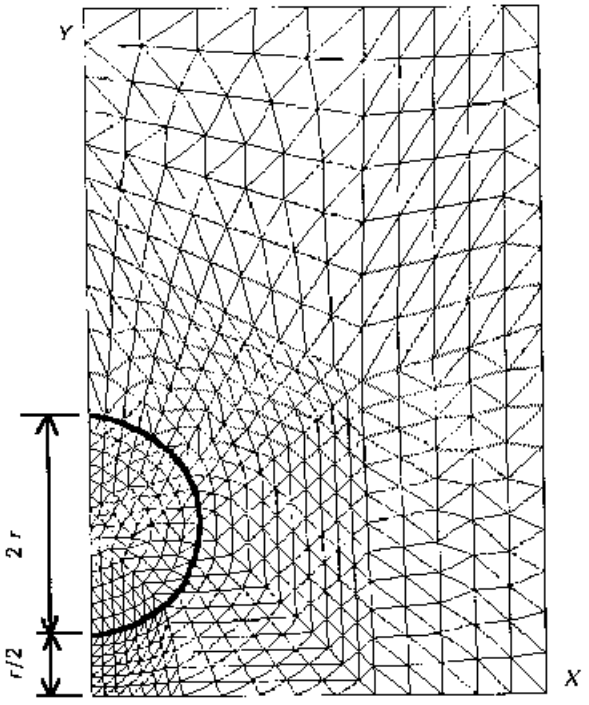

Figure 2 Mesh used to compare the strains obtained with finite element (axisymetric 6 node triangles, 1818 nodes) with those obtained with the present technique.

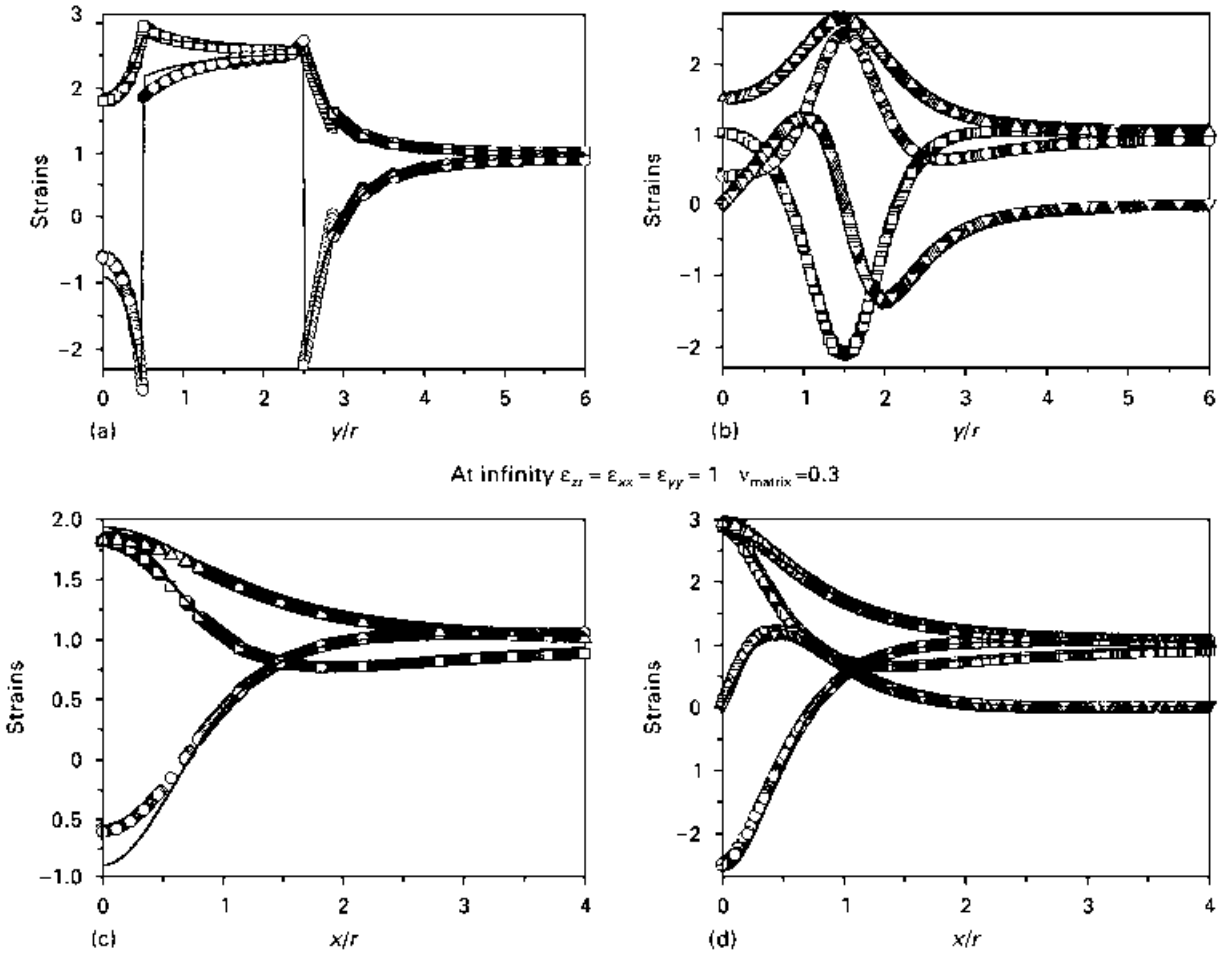

Figure 3 Strains along four axes for the geometry of Fig. 2: (a) $x = 0$, (b) $x = r$, (c) $y = 0$, (d) $y = r/2$. The results from finite element (symbols) are compared to those from the present technique (lines): (□) e_{xx}, (○) e_{yy}, (∇) e_{xy}, (△) e_{zz}.

radius for spheres of the same radii to avoid any significant error of more than 10% in comparison with the applied load.

3. Preparation of macroporous epoxies via chemically induced phase separation (CIPS)

3.1. Materials

Bisphenol A diglycidylether (DER332 from Fluka) and 2,2-bis(4-amino-cyclohexyl) propane (HY2954 from Ciba-Geigy) were used as the precursors to build the epoxy network. Cyclohexane was purchased in analysis grade.

3.2. Experimental procedure

Macroporous epoxies were prepared according to the chemically induced phase separation technique as described below. First, the bifunctional epoxy precursor was mixed at room temperature with the tetrafunctional diamine in a stochiometric ratio of 2 : 1 together with the desired amount of cyclohexane. This homogeneous mixture was transferred into glass tubes, 5 mm diameter, which were sealed at one end and immersed into liquid nitrogen. This system was then connected to a vacuum pump. A closed system was realized by sealing the tube at the other end with a heating gun. The tube was consequently removed from the liquid nitrogen and allowed to heat in a silicone oil bath at 60°C, thus allowing for effective homogenization. The closed tubes were then put in a preheated oven and cured at $T = 80\,^{\circ}\mathrm{C}$ for 16 h. The samples were then removed out of the glass tubes and heated stepwise at $20\,\mathrm{K\,h^{-1}}$ to 200 °C for an additional 120 h to allow for complete solvent removal and full cure.

3.3. Characterization methods

The sample morphology has been investigated with scanning electron microscopy on a Cambridge S100 at an accelerating voltage of 10 kV. The samples were immersed in liquid nitrogen and then fractured with a razor blade (to avoid plastic void growth, otherwise resulting in a change of the size and shape of the voids) and the fracture surfaces were coated with gold, approximately 100 nm thick, with a Bio Rad coating apparatus.

The mechanical studies were performed on cylindrical samples of 5 mm diameter and around 15–20 mm in length, machined from the macroporous epoxies. These specimens were tested under compression on a UTS 100 universal testing machine with a constant deformation rate of $10^{-4}\,\mathrm{s^{-1}}$.

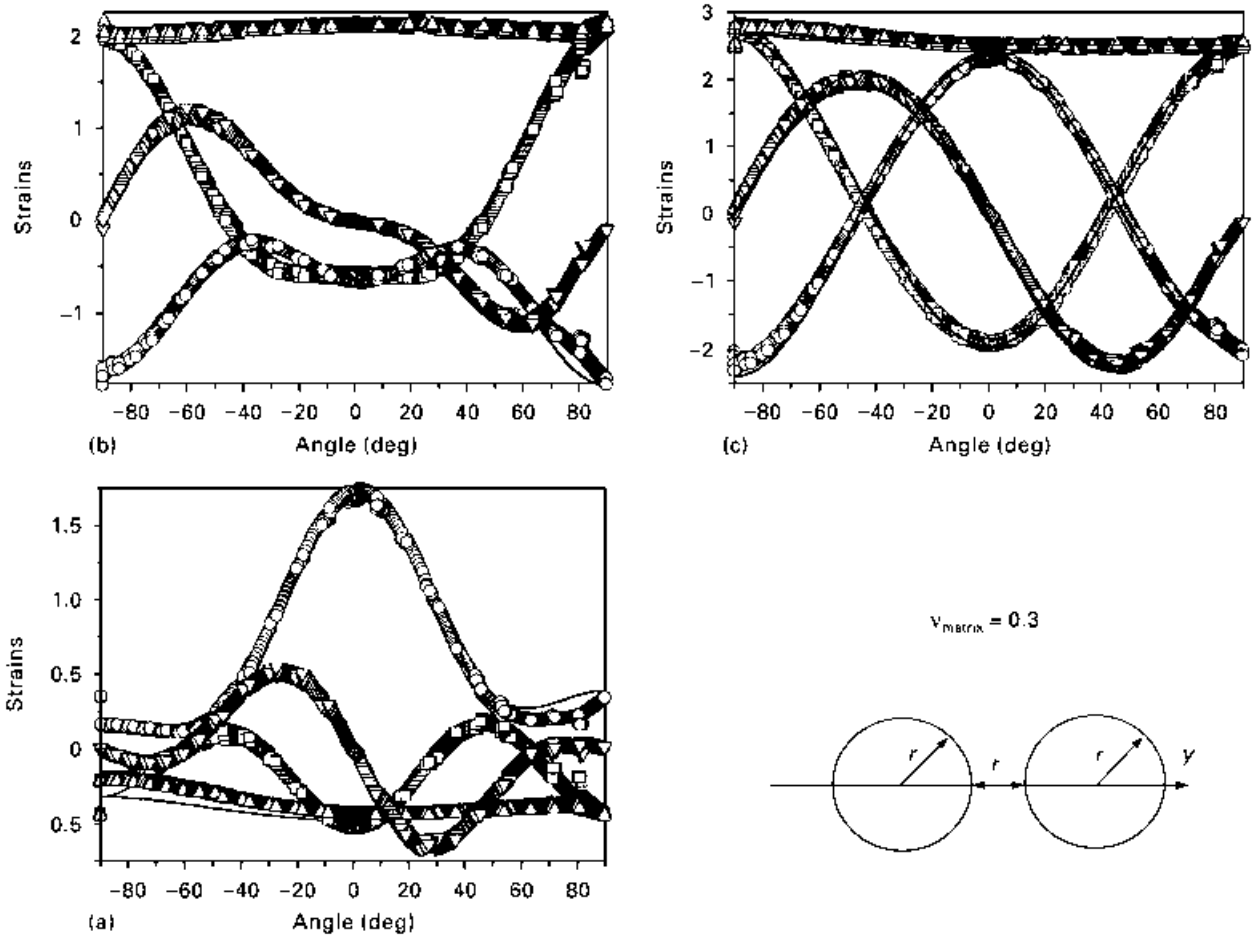

Figure 4 Strain around a void for the geometry of Fig. 2 and for (a) uniaxial, (b) biaxial and (c) triaxial tension. The results from finite element (symbols) are compared to those from the present technique (lines). (□) e_{xx}, (○) e_{yy}, (△) e_{zz}, (▽) e_{xy}.

4. Application of the zero-order strain interaction model to porous materials

4.1. Spatial distribution of spheres

We considered in our computations an infinite matrix containing voids of the same radii. Each centre of a void of radius r was randomly placed (by a computer) in a definite volume, in respect of a minimum distance $l_{min} = r$ to the voids placed before. In order to avoid border effects, only a central volume of the total void containing volume was treated with detailed calculations. The volumes were of cubical form consisting of the central cube, the inner cube and the external cube as shown in Fig. 5. In fact, a "margin" of $10r$ was necessary to simulate an infinite medium for the border voids (interacting with the voids located outside the cube c in Fig. 5) of the central cube, thus forming the inner cube. A supplement "margin" of $5r$ was necessary to avoid the border effects due to the random distribution leading to the external cube. Indeed, if spheres are randomly placed in a finite volume, the local volume fraction will alter slightly inside the cube. As the volume fraction is zero outside the cube, it becomes easier to place spheres near the border. Consequently, this leads to a locally higher volume fraction in the external cube.

We have examined several distributions, and found that a distance $5r$ was sufficient practically to render the distribution random inside the central cube and to overcome the border effects. Thus it became possible to simulate random distributions with up to 150 spheres. For the typical example of Fig. 6, the central cube contained 138 voids of radius r in a volume of $(18r)^3$, which gives a volume fraction of pores, of 9.94%. The inner cube of interactive voids of volume $(38r)^3$ contained 1292 voids and the external cube of volume $(48r)^3$ contained 2613 voids. Because of the minimum distance $l = r$ separating voids owing to the weakness of the zero-order approximation, we were not able to simulate a higher volume fraction of voids (typically more than 10%). It is clear from Fig. 6, where the six faces of the central cube are shown, that the particles display a random distribution and that there are many spheres at a distance of l_{min} to $1.1l_{min}$ from the nearest neighbour sphere. The mean sphere inter-distance is $1.13r$.

4.2. Distance of mechanical interaction

It is obviously impossible to take into account an infinite number of inhomogeneities in a single computation by using Equation 1. Each inhomogeneity gave rise to a particular computation. The number of problems to solve was the same as the number of inhomogeneities in the central cube. The computation concerning a reference void involved all the voids located in a sphere of radius d centred at the reference

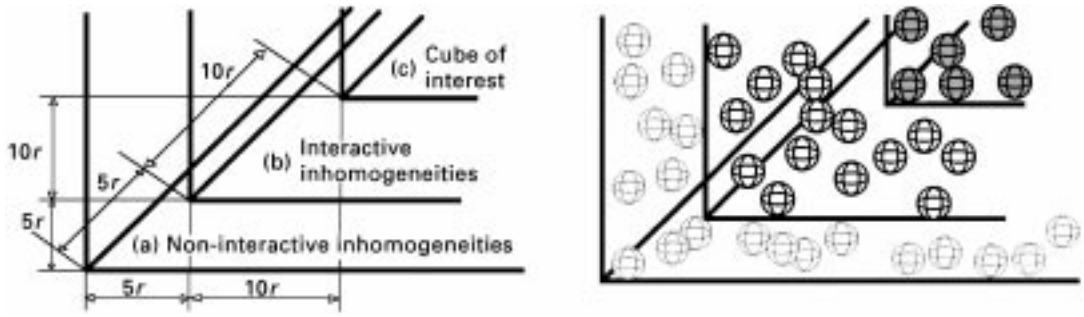

Figure 5 Schematic representation of the three volumes containing spheres of different interest: (a) volume excluded to avoid border effect of the random distribution in a finite volume, (b) volume containing inhomogeneities taken into account in the interaction computations, and (c) volume where the strains inside each inhomogeneity are computed.

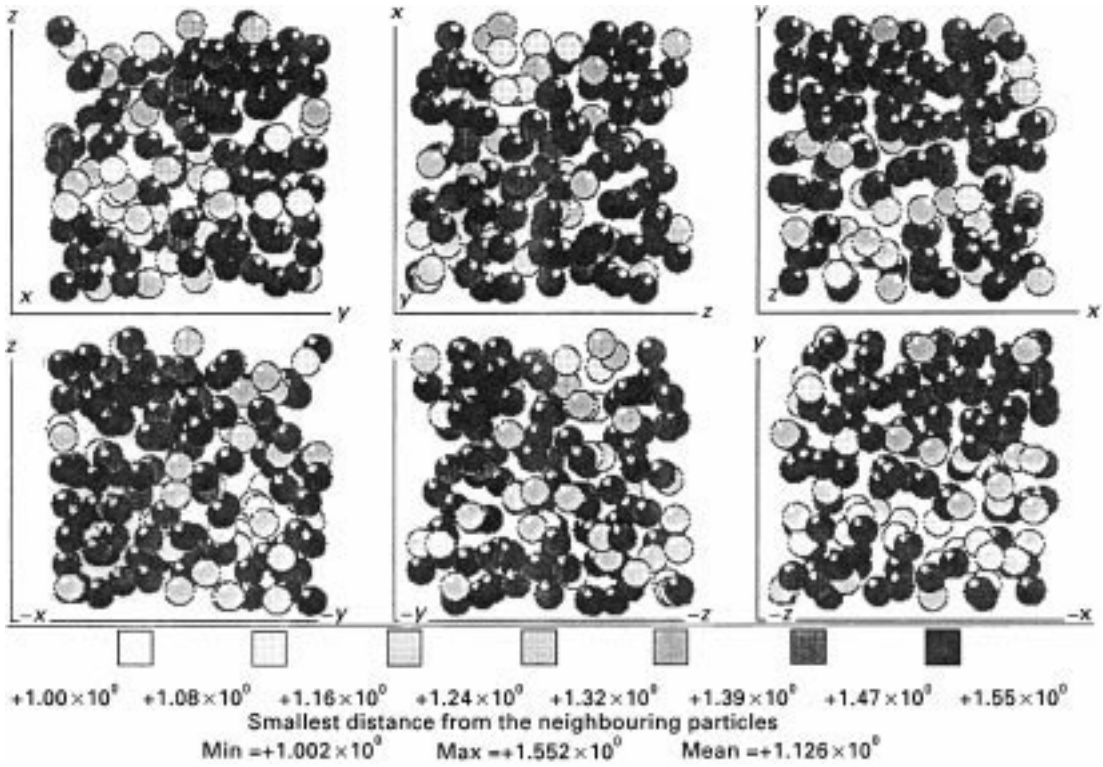

Figure 6 Typical example of the distribution of 138 spheres contained in a cube. The six faces of the cube are visualized and the darkness of the spheres indicates the proximity of the nearest sphere.

(Fig. 7). The distance d (centre to centre) of active interaction was chosen by the user. The limits of our computers (computation time and memory size) did not allow us to use values of d greater than typically $10r$.

We varied the distance d from $3r$ to $10r$. The solution obtained for $10r$ was taken as reference. We compared the differences between the ε_i^p relative to the maximum component of the applied strain tensor at infinity. The loading was always a uniaxial tension along the z axis. The difference, Δ, with respect to the reference solution is then

$$\Delta = \max i\{[\varepsilon_i^p(d) - \varepsilon_i^p(10r)]/\varepsilon^{zz}\} \qquad (2)$$

where $\varepsilon_i^p(d)$ is the solution obtained for the inhomogeneity p with an active interaction distance d. The maximum is searched over the six components of the strain tensor and the total number of inhomogeneities. The plot of Δ versus d/r in Fig. 8 indicates that $\Delta < 5\%$ when $d/r > 8$. We then considered that d/r should be greater than 8 to take into account the most significant interactions. One can

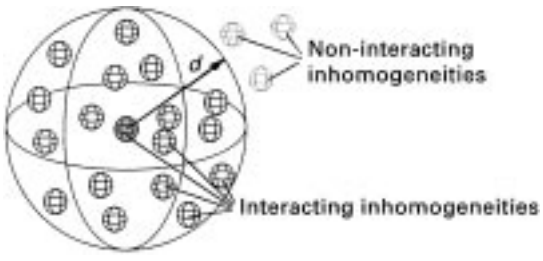

Figure 7 Schematic representation of the sphere inside which all inhomogeneities interact with each other and with the reference sphere to compute the strains of the homogeneity located at the centre.

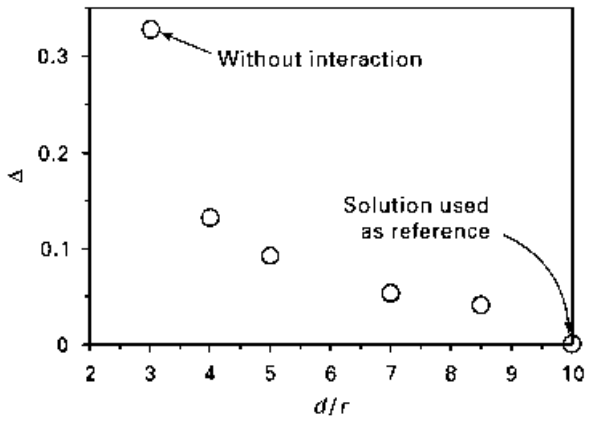

Figure 8 Evolution of the solution versus the active interaction distance d.

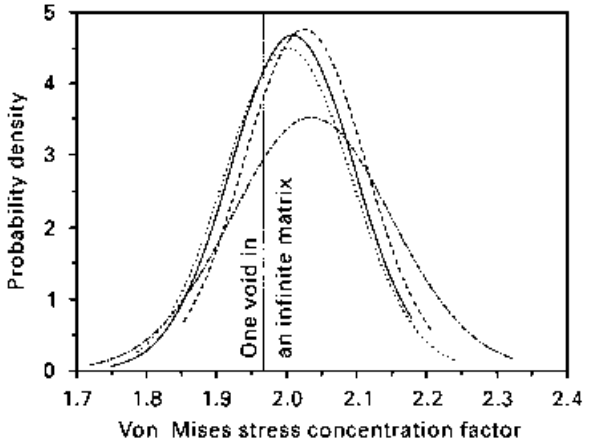

Figure 9 Statistical distribution of von Mises stress concentration factors (—) 87 voids, (----) 100 voids, (——) 100 voids, (– · –) 138 voids.

also conclude that for our spatial distributions ($l_{min} = r$, $v^r < 10\%$) a void does not interact with others located at a distance greater than approximately $10r$.

4.3. Distribution of stresses in porous materials

In porous materials, the presence of voids induces stress concentrations. In many polymers, plasticity or crazing develop at the vicinity of inhomogeneities and in porous polymers voids can grow and coalesce. It was then our purpose to analyse the appearance of plasticity and the consequences of the interactions between voids on the stress concentrations. The appearance of plasticity is generally well described by a von Mises criterion in these materials. For the sake of simplicity, the dependence of the yield criterion on the hydrostatic stress is neglected. Thus, it was possible to compute the stresses around the particles to find the maximum von Mises equivalent stress, τ_e. The location of the maximum value of τ_e was searched around the particle with an accuracy in angle of 1°. Fig. 9 shows the statistics of the distribution of τ_e. It is noticeable that the mean value of the stress concentrations is a few percent greater than the exact value for a single void in an infinite matrix [39, 43]. The effect of mechanical interaction globally increases τ_e and the appearance of plasticity is encountered for a lower external loading. Practically, the yield stress of the material decreases when interaction is present.

The numerical simulations of the stress distibutions were carried out on porous materials submitted to uniaxial tension. We have chosen a high value for the interaction distance, d, thus allowing the multiple

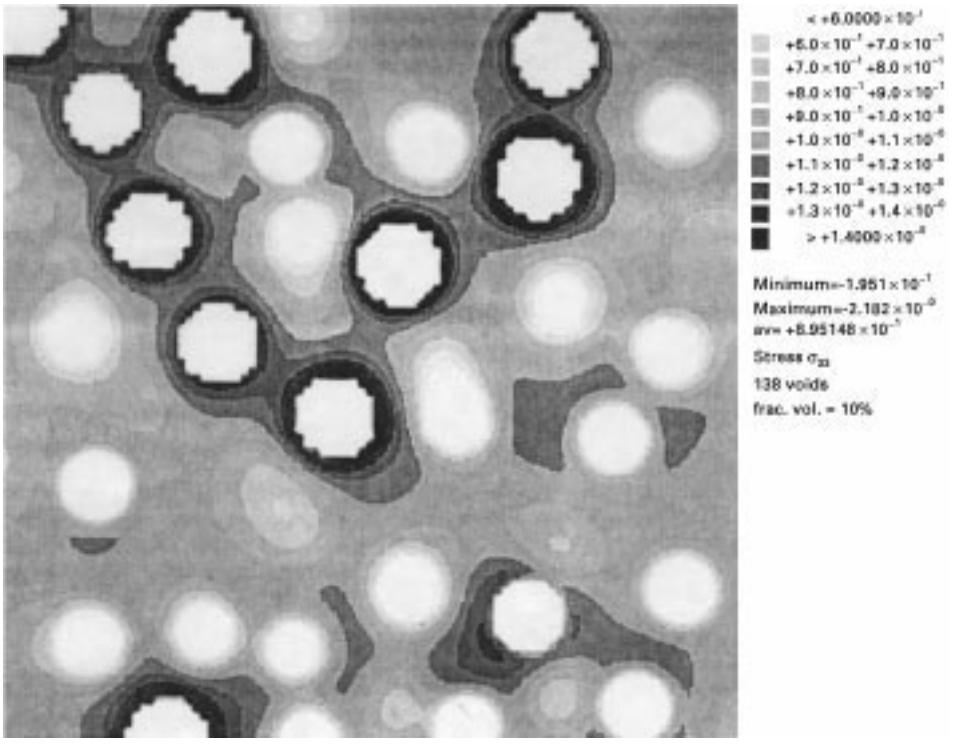

Figure 10 Stress distribution of σ_{33} at a constant value of z for a sample containing 138 voids subjected to a tensile deformation of 1%.

interaction of voids to be taken into consideration and to minimize the difference to the reference solution as discussed above. A typical example of the stress distribution in the z-direction, σ_{33}, at a constant value of z is shown in Fig. 10 for a sample containing 138 voids subjected to a deformation of 1%. Clearly, a large number of points is observed, where the stress is completely released. These points correspond to locations, where a void can be found either closely below or above the plane at the considered value of z. This picture also demonstrates the importance of the interaction of voids on the stress concentrations. If the distance between two neighbouring pores, is large, no increase in stress concentration is observed. However, if several voids are located very close to each other, the interaction leads to the build-up of internal stresses, which are considerably higher than the imposed loading. This observation is also confirmed, if one plots the normalized von Mises stresses, for the same conditions (Fig. 11). Again, a large number of points can be recognized, where the stress is released and, on the other hand, a considerable number of regions is seen where the von Mises stress becomes twice the value of the external loading. Those regions will lead to an effective lowering of the onset of plastic deformation, representing the yield point. The calculations predict the plasticity to appear locally for macroscopic loadings which are by a factor of about 1.7–2.3 lower than the yield stress of the neat matrix. The normalized distribution of stress concentration seems to be insignificantly influenced by the volume fraction of pores in the range 2%–10%. The volume fraction of pores is obviously related to the total volume of plastically deformed material.

5. Discussion of experimental results and theoretical predictions

In order to check the validity of the numerical simulations, we have prepared porous epoxies via the chemically induced phase separation (CIPS) technique. This results in the formation of a closed porosity with a narrow pore-size distribution centred around 1.5–5 μm diameter depending on the initial solvent concentration. The phase separation proceeds via a nucleation and growth mechanism and not via spinodal decomposition [32]. Thus the domains tend to take the shape which offers the highest volume to surface ratio. Therefore, the pores are nearly spherical, as it can be clearly seen from Fig. 12, which shows scanned electron micrographs of macroporous epoxies prepared via CIPS with different amounts of cyclohexane. It can be clearly seen, that the macroporous epoxies display a very narrow size distribution. The statistical distribution of the voids coincides with the random distribution of the model system.

The structural characteristics can be controlled over a wide range depending on the curing temperature, the chemical nature of the solvent and its concentration [32]. For our experiments, we have chosen cyclohexane as the solvent and kept the curing temperature constant. Consequently, the morphological characteristics depend only on the initial solvent concentration. At a curing temperature of 80 °C, a phase separation resulting in the formation of white, opaque samples is observed at concentrations equal to or higher than 16 wt % cyclohexane. Only part of the initial solvent is involved in the phase separation process. A considerable amount remains soluble in the cross-linked material. An increase in solvent

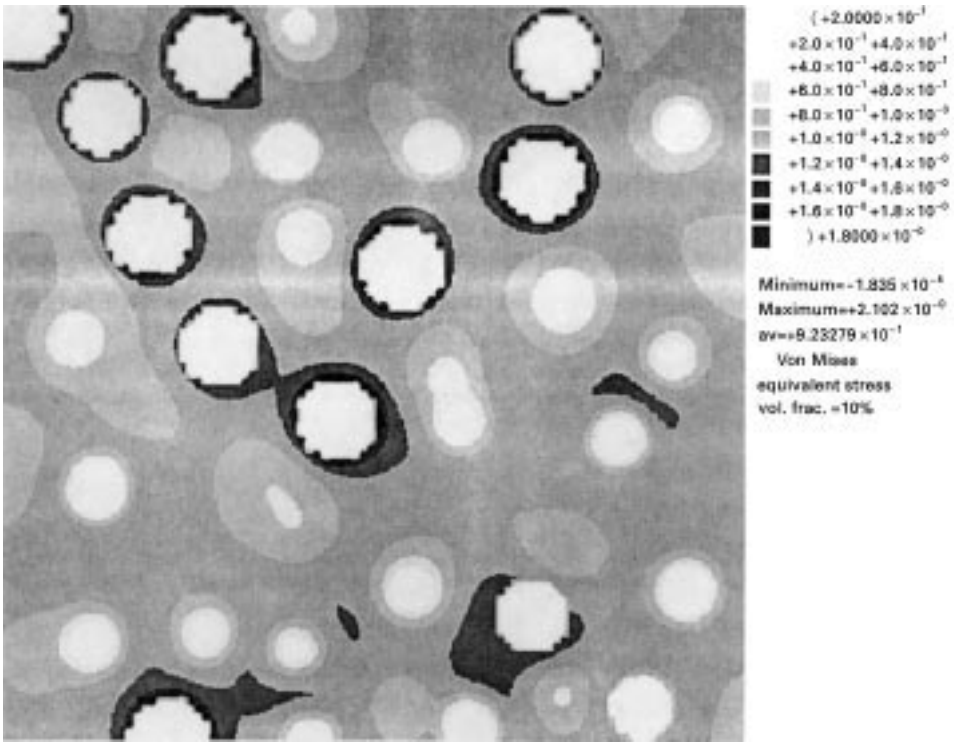

Figure 11 Von Mises stress distribution at a constant value of z for a sample containing 138 voids subjected to a tensile deformation of 1%.

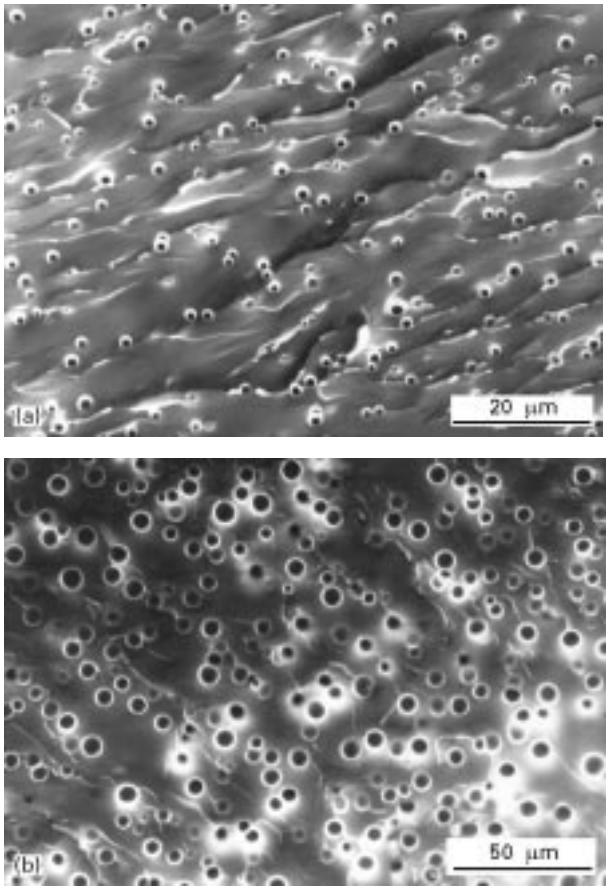

Figure 12 Scanning electron micrographs of macroporous epoxies prepared via chemically induced phase separation with various amounts of cyclohexane: (a) 16 wt % cyclohexane, (b) 20 wt % cyclohexane.

concentration leads to an increase in the pore size and also in the volume fraction as can be clearly seen from Fig. 12. The structural characteristics such as pore size, inter-pore distance (IPD) and volume fraction are reported in Table I. The porosity has been determined from density measurements after the drying procedure. The drying was performed by heating the samples above the ultimate T_g and the complete drying has been checked by thermogravimetric analysis.

Typical results of stress deformation curves under uniaxial compression of the neat matrix material and a porous epoxy prepared with 20% cyclohexane, thus exhibiting a porosity of around 13%, are plotted in Fig. 13. In these curves, three different regions can be mainly distinguished. In the early stage of deformation the material shows an ideally linear behaviour. The modulus, given by the slope in this early stage of deformation, decreases as a consequence of the generation of a porous morphology. The onset of plastic deformation leads to a deviation from the linear behaviour. It is concluded from the zero-order model that the shear banding starts at a limited number of voids ($< 5\%$), which satisfy the yielding criterion. As the external load increases further, in the second region, the stress concentrations in the material become more important, involving a continuously increasing number of pores to fulfill the yielding criterion. As the stress concentrations exceed the yield stress in the entire material, extensive plastic deformation takes

TABLE I Morphological characteristics of macroporous epoxies used for compression testing

Cyclohexane (wt%)	Density after drying (g cm^{-3})	Porosity (%)	Pore diameter (μm)	IPD (μm)
0	1.123	–	–	–
16	1.1	2.05	1.3	2.5
18	0.982	12.6	4.4	2.7
20	0.975	13.2	4.9	2.9
22.5	0.935	16.7	5.3	2.4
25	0.94	16.3	6.6	3.1

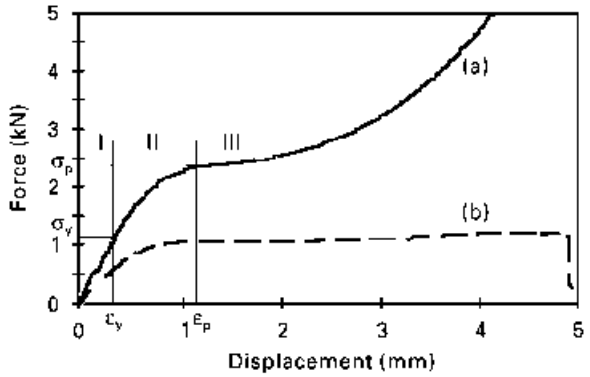

Figure 13 Load–displacement curves under uniaxial compression for (a) the next epoxy and (b) macroporous epoxy prepared via CIPS with 20 wt % cyclohexane.

place in region 3. Our calculations were limited to the elastic behaviour. Therefore, in the following discussion, the onset of plastic deformation will be taken as a comparative value for the yield strength, σ_y and not the stress at the onset of extensive plastic deformation, σ_p. Fig. 14 shows the experimental data of the yield strength, σ_y, as well as σ_p in comparison to the values calculated from the zero-order model. Even though the concentration of solvent has been varied stepwise with steps of 2%, a drastic difference in porosity is obtained for samples prepared with 16 and 18 wt % cyclohexane. Thus, for this particular system, no porous epoxies could be prepared with the CIPS technique with porosities in the range of 2%–10%. On the other hand, the calculations were limited to 10% porosity. The calculations based on the zero-order model, with the restriction of a separating distance between voids of at least one radius, predict a decrease in yield strength to around 45%–55% of the value for the neat matrix independent of the degree of porosity. The experimental values for the yield strength, taken as the first point of deviation from the linear behaviour, as discussed above, are somewhat higher than the predicted values. However, if one compares the strength at the onset of extensive massive plastic deformation, σ_p, to the theoretical predictions, it is confirmed, that the theoretical and experimental values are in good agreement (Fig. 14).

On-going work is dedicated to improve further our micromechanical model for simulation of several interesting morphologies, such as bimodal pre-size distributions and compare these results with data

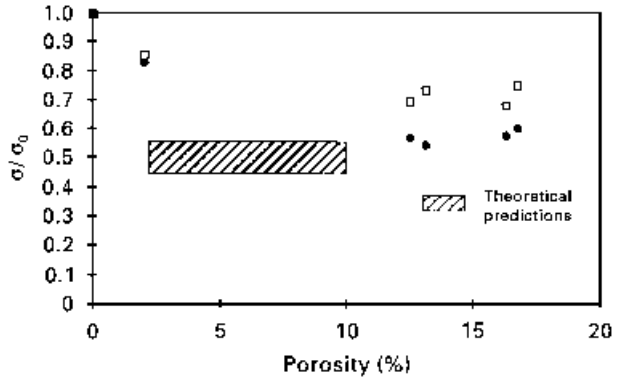

Figure 14 Comparison of theoretical predictions and experimental results for the lowering of yield strength, σ_y, and stress at the onset of extensive plastic deformation, σ_p, obtained from macroporous epoxies prepared via CIPS and related to the values of the neat matrix, σ_{y0} and σ_{p0}. (●) σ_p/σ_{p0}, (□) σ_y/σ_{y0}.

obtained from tensile tests on macroporous epoxies exhibiting morphologies in better agreement with the calculations. The *equivalent inclusion method* [40] represents a possible way to minimize the separatingdistance between voids, thus rendering the simulation closer to the real morphology.

5. Conclusion

The spatial distribution of inhomogenities such as voids is a key parameter for the material toughness modification. A technique based on Eshelby's model has been proposed to analyse the effects of mechanical interaction on the onset of yielding in a porous material. It has been shown that the mean stress concentration factor is greater than that obtained for an isolated void owing to the multiple interactions. These theoretical predictions are in agreement with experimental results obtained on porous epoxies prepared via the chemically induced phase separation technique, thus exhibiting a morphology similar to the model used for the calculations. However, as the present model did not allow a separating distance between voids smaller than one radius of a void, it is expected, that the calculated mean values are lower than those which would be obtained for a random distribution of voids without the restriction of a separating distance. Therefore, a refined model based on the *equivalent inclusion method* will be developed.

References

1. R. BAGHERI and R. A. PEARSON, *in* "*25th International SAMPE Technical Conference*" (1993) pp. 25–39.
2. R. A. BUBECK, D. J. BUCKLEY, E. J. KRAMER and H. R. BROWN, *J. Mater Sci.* **26** (1991) 6249.
3. C. B. BUCKNALL, V. L. P. SOARES, H. H. YANG and X. C. ZHANG, *Macromol. Symp.* **101** (1996) 265.
4. K. DIJKSTRA, A. VAN DER WAL and R. J. GAYMANS, *J. Mater Sci.* **29** (1994) 3489.
5. D. DOMPAS, G. GROENINCKX, M. ISOGAWA, T. HASEGAWA and M. KADOKURA, *Polymer* **35** (1994) 4750.
6. Y. HUANG, D. HUNSTON, A. J. KINLOCH and C. RIEW, *Adv. Chem. Ser.* **233** (1993) 1.
7. A. LAZZERI and C. B. BUCKNALL, *J. Mater Sci.* **28** (1993) 6799.
8. J. P. PASCAULT, *Macromol. Symp.* **93** (1995) 43.
9. R. SCHIRRER and C. FOND, *Rev. Metall. Cah. Inf. Techn.* **92** (1995) 1027.
10. A. F. LU, Thesis no. 1391, Swiss FederalInstitute of Technology (1995).
11. C. K. RIEW and J. K. GILLHAM, "Rubber-modified thermoset resins", *Advances in Chemistry Series*, Vol. 208 (1984).
12. C. K. RIEW, "Rubber toughened plastics", *Advances in Chemistry Series*, Vol. 222 (1989).
13. C. K. RIEW and A. J. KINLOCH, "Toughened Plastics: Science and Engineering", *Advances in Chemistry Series*, Vol. 233 (1993).
14. A. A. COLLYER, "Rubber toughened engineering plastics" (Chapman and Hall, London 1994).
15. B. J. CARDWELL and A. F. YEE, *ANTEC* (1995) 1519.
16. C. A. CRUZ JR and S. HAVRILIAK JR, *ibid.* (1995) 1521.
17. Y. HUANG and A. J. KINLOCH, *Polymer* **33** (1992) 1330.
18. L. BOOGH, B. PETTERSON, S. JAPON and J. A. MÅNSON, *in* "*Proceedings of ICCM*", Vol. 10 (1995) pp. 389–96.
19. H. J. SUE, *J. Mater. Sci.* **27** (1992) 3098.
20. C. B. BUCKNALL, A. KARPODINIS and X. C. ZHANG, *ibid.* **29** (1994) 3377.
21. R. SCHIRRER, C. FOND and A. LOBBRECHT, *ibid.* **31** (1996) 6409.
22. C. FOND and R. SCHIRRER, *Int. J. Fract.* **77** (1996) 141.
23. R. BAGHERI and R. A. PEARSON, *Polymer* **36** (1995) 4883.
24. *Idem*, *ibid.* **37** (1996) 4529.
25. Y. HUANG and A. J. KINLOCH, *J. Mater. Sci. Lett.* **11** (1992) 484.
26. D. LI, A. F. YEE, I. W. CHEN and K. TAKAHASHI, *J. Mat. Sci.* **29** (1994) 2205.
27. S. WU, *J. Appl. Polym. Sci.* **35** (1988) 549.
28. A. MARGOLINA and S. WU, *Polymer* **29** (1988) 2170.
29. J. KARGER-KOCSIS, *Polym. Eng. Sci.* **36** (1996) 203.
30. *Idem*, *Polym. Bull.* **36** (1996) 119.
31. J. KIEFER, J. G. HILBORN, J. A. E. MANSON, Y. LETERRIER and J. L. HEDRICK, *Macromolecules* **29** (1996) 4158.
32. J. KIEFER, J. G. HILBORN and J. L. HEDRICK. *Polymer* **37** (1996) 5715.
33. J. KIEFER, R. POROUCHANI, D. MENDELS, J. B. FERRER, C. FOND, J. L. HEDRICK, H. H. KAUSCH and J. G. HILBORN in "Microporous and macroporous materials", *MRS Symposium Proceedings*, Vol. 431 (1996) 527–32.
34. J. KIEFER, R. POROUCHANI, D. MENDELS, J. B. FERRER, C. FOND, J. G. HILBORN and H. H. KAUSCH, *Oberflächen Werkstoffe* **5** (1996) 12.
35. J. KIEFER, H. H. KAUSCH and J. G. HILBORN, *Polym. Bull.* **38** (1997) 477.
36. Y. HUANG and A. J. KINLOCH, *J. Mater. Sci.* **27** (1992) 2763.
37. F. J. GUILD and A. J. KINLOCH, *ibid.* **30** (1995) 1689.
38. J. D. ESHELBY, *Proc. R. Soc. Lond.* **241A** (1957) 376.
39. *Idem*, *ibid.* **252A** (1959) 561.
40. Z. A. MOSCHOVIDIS and T. MURA, *J. Appl. Mech.* **42** (1975) 847.
41. N. M. FERRERS, *J. Pure Appl. Math.* **XIV** (1877) 1.
42. F. W. DYSON, *ibid.* **XXV** (1891) 259.
43. J. N. GOODIER, *ASME Trans.* **55** (1933) 39–44.

Received 10 March 1997
and accepted 2 April 1998